Iranian Journal of Chemical Engineering
Vol. 9, No. 2 (Spring), 2012, IAChE

Manganese Oxide Promoted $LaCoO_3$ Nano-Perovskite for Oxidation of a Model Exhaust Gas

S. Farhanian Moghadam[1], A. Malekzadeh[1], M. Ghiasi[1], F. Karimi[1], Y. Mortazavi[2], A. Khodadadi[2]*
1- School of Chemistry, Damghan University (DU), Damghan, I. R. Iran.
2- School of Chemical Engineering, University of Tehran, Tehran, I. R. Iran.

Abstract

Catalysts with the formula of $LaCoMn_xO_{(3+\delta)}$, where x *is 0.0, 0.2, 0.3 and 0.5 were studied for CO and C_2H_6 oxidation. Ethane was selected as a model for hydrocarbon combustion. Samples were prepared by the citrate method and calcined at 600°C for 8 h. Prepared catalysts were characterized by FT-IR, XRD, SEM, TEM, TPR and EDS analyses. Structural studies show that the manganese oxide addition up to 0.5 mol, i.e. 50%, has no effect on the $LaCoO_3$ perovskite phase formation. Crystallite size of different phases, comprising perovskite and manganese oxide, was determined by the Scherrer equation. Addition of 0.3 mol manganese was observed to improve the catalytic property of the lanthanum cobaltite; oxidizes the CO and hydrocarbons at lower temperature.*

Keywords: *Mixed Oxides, $LaCoO_3$, Manganese Oxide, CO Oxidation, Hydrocarbon Oxidation, Perovskite*

1. Introduction

Poisonous components such as carbon monoxide, observed to be in the automotive exhaust gas, exit from the engine. These harmful components are converted to inert gases, such as carbon dioxide in catalytic converters, before the exhaust gas is emitted to the atmosphere [1]. The catalytic converters are, in fact, reactors that consist of monolithic honeycomb skeletons, made of ceramic or metallic materials [1]. This structure is then coated by a ceramic substrate impregnated with platinum group metals (PGM) as the active catalytic sites. However, due to the rising cost of PGM, many researchers have been searching for alternative materials as the active catalytic phase .

Perovskite group of materials with a general formula of ABO_3 in which A and B are cations of different sizes, are known as one of the most promising active phases for the environmental applications. The catalytic properties of perovskite type oxides basically depend on the nature of A and B ions [1]. The A site ions are catalytically inactive. The nature of these ions, however, also influences the stability of the perovskite phase. Replacement of part of A or B ions with other heterovalent ions can induce structural

* Corresponding author: malekzadeh@du.ac.ir

modifications that may generate oxygen vacancies and/or change the valence state of the original cations [1]. Lanthanum cobaltite, $LaCoO_3$, belongs to a family of mixed electronic and oxide-ion conducting perovskites that are good candidate materials for catalysts, oxygen separation membranes, solid oxide fuel cell cathodes, and oxygen sensors [2]. In particular, partial substitution of La with divalent ions, e.g. Sr^{2+}, increases the average oxidation state of the cation in position B, which is Co cation [1].

Cobalt containing perovskite type oxides have received great attention due to their interesting application properties [3]. It has been pointed out that the important role of the lattice distortions, generated by A-site substitution in perovskites, is on their structural and catalytic properties. Partial substitution of the A ion by another of a lower oxidation state may induce important changes in stability [3]. Perovskites are well known catalysts for numerous oxidation reactions. These include total and partial oxidation of methane and carbon monoxide oxidation [4]. The perovskite structure is very versatile and can stand many crystalline defects.

Noble metal based catalysts are more preferred because of their high activity in complete ethanol combustion than those containing base metal oxides. However, noble metals are expensive and sensitive to poisons. Manganese oxides have been reported as an active catalyst for oxidation, among others, of methanol and ethanol. Manganese oxides are compounds with a typical berthollide structure that contain labile lattice oxygen. Their catalytic properties are attributed to their oxygen storage capacity in the crystalline lattice which is due to the capacity of manganese to form oxides with variable oxidation states (MnO, Mn_2O_3, MnO_2 or Mn_3O_4). According to the labile oxidation state, Mn is capable of playing the role of either a reducing agent (Mn^{2+} - e $\rightarrow$ Mn^{3+} - e $\rightarrow$ Mn^{4+}) or an oxidizing agent (Mn^{4+} +e$\rightarrow$$Mn^{3+}$+e$\rightarrow$ Mn^{2+}), acting in both cases as an active component of the redox system [5]. MnO_2 and Mn_2O_3 were identified as the catalytically active components; the ratio between both of these oxides is a function of Mn loading (dispersion), temperature of catalyst treatment during preparation, method of preparation and Mn precursor [6]. Low cost of MnO_x is in contrast to the expensive noble metal catalysts. With the growing demands of innovative technology, manganese oxides based catalysts may find a new application. Supported and unsupported manganese oxides have been found to be active for the various catalytic reactions such as oxidation of carbon monoxide, methane, hydrocarbons and are also found active for the decomposition of ozone, N_2O, H_2O_2, the selective catalytic reduction of NO and the removal of hydrogen sulfide [7-14]. Mixed oxides of Mn such as Mn/ceria and Mn/copper oxide were also found to enhance the catalyst activity during the CO oxidation and SCR of NO, respectively [15-16].

The structural transformation of MnO_x depends on the calcination temperature during pretreatment. Thus, low calcination temperature and low Mn loading led to formation of more MnO_2 phase, whereas high Mn loading and calcination

temperatures favored formation of Mn_2O_3 or Mn_3O_4 phases [17-19].

This work is directed to study the manganese oxide added lanthanum cobaltite toward the oxidation of a model exhaust gas, comprising the CO and C_2H_6 component. The relationship between the structure, redox properties and dispersion of the MnO_x on the $LaCoO_3$ and catalytic property is understood by the characterization techniques of the X-ray diffraction (XRD), scanning electron microscopy (SEM), fourier transform infrared spectroscopy (FT-IR) and hydrogen temperature-programmed reduction (H_2-TPR) analyses.

2. Experimental

Samples of $LaCoMn_xO_{(3+\delta)}$, where x is 0.0, 0.2, 0.3 and 0.5 were prepared by the citrate method in a way almost identical to that reported by L. Abadian et al. [20]. A solution with appropriate moles of the corresponding metal nitrates and citric acid equivalent with nitrate ions moles was evaporated at 80°C overnight. The obtained spongy, friable material was subsequently dried at 150°C overnight. The resulting material was powdered and kept at 200°C overnight. The resulting brown material was completely powdered and calcined at 600°C for 8 h. The crystal structures of the fresh catalysts were determined by X–ray powder diffraction (XRD) method in a Philips Xpert MPD diffractometer using Cu-Kα (λ=1.54056 Å) radiation filtered by a copper tube, operated at 50 KV and 40 mA. Diffraction patterns were recorded in the 2θ range of 20 – 90° at a scanning rate of 0.02° (2θ)/min. The average crystallite size was calculated by applying the Scherrer equation on the reflection [21-23]. Scanning electron microscopy (SEM) and energy dispersive X-ray micro analysis (EDX) were done by a Philips XL30 instrument to investigate the particle size and morphology as well as the elemental composition of the catalysts. Transmission electron microscopy (TEM) image was obtained on a Philips XL30 transmission electron microscope with an accelerating voltage of 100 kV. H_2-temperature programmed reduction (TPR) tests were carried out using a Quantachrome CHEMBET-3000 apparatus. The TPR experiments were performed on 0.020 g of perovskite samples by 10 cm^3 STP/min of 7.0% H_2 in Ar. Temperature was raised from 100 to 950°C with a heating rate of 10°C/min. FT-IR spectra were recorded in a Perkin-Elmer spectrum RXI-IR spectrometer, operating in ratio, single-beam, or inter-frogram mode, in the range of 400–1600cm^{-1}. The samples were finely ground in an agate mortar with KBr as diluent and pelleted for the IR analysis. The catalytic activity of the samples was studied using a model exhaust gas containing a mixture of 6.0% CO and 0.2% C_2H_6, as a hydrocarbon (HC) model compound, in Ar. A schematic of the experimental set-up and the reactor is shown in Fig. 1. The flow rates of the model gas mixture and air were set by mass flow controllers in order to obtain a synthetic exhaust gas with total flow rate of 47 cm^3 STP/min and $\lambda = 1$. Here λ is the stoichiometric number with the definition of $\lambda = \frac{(\text{Air/Fuel})_{\text{Actual}}}{(\text{Air/Fuel})_{\text{Stoichiometric}}}$. Oxidation of the synthetic exhaust gas pollutants was studied in a fixed bed micro-reactor (5mm × 300mm) at atmospheric pressure. All the perovskite samples were pelleted, crushed and sieved to

particle size of 80–120 mesh size. The amount of 200 mg of each perovskite (~4mm in height), supported on a small amount of ceramic wool (~ 3mm in height), was used for measuring oxidation activities of the catalysts. The reactor temperature was raised in a tubular furnace (70 mm) by a temperature controller. A thermocouple, attached to the outer wall of the reactor, was used for both monitoring and controlling the temperature of the reactor. Concentration of the effluents was analyzed by a gas chromatograph equipped with a methanizer and FID. Also, a set of valves allowed bypassing the reactor feed and provided a direct measurement of the pollutants concentrations in the feed by the gas chromatograph. For conversion measurements versus temperature, concentration of the effluents was analyzed after steady state was achieved at the desired temperature. The temperature was then increased to the next level and again after steady state was reached, analysis of the reaction products was performed. This procedure was repeated for the whole temperature range, i.e. 70–650°C, used in this investigation. No carbon dioxide was detected using an empty reactor equipped with the ceramic wool.

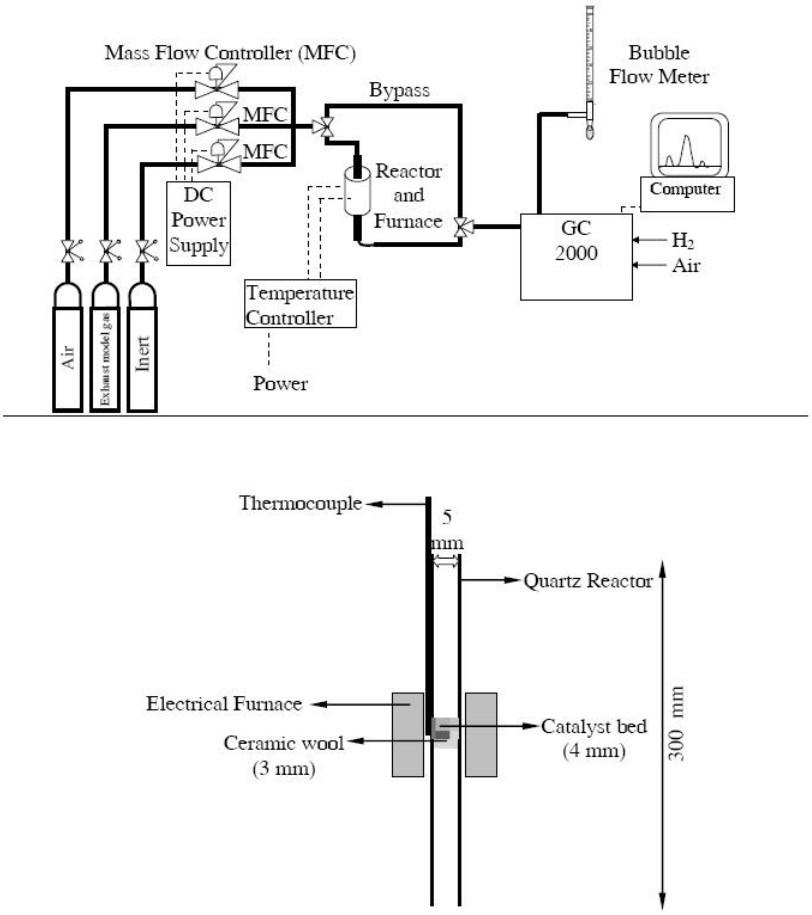

Figure 1. Schematic of the set-up and reactor

3. Results and discussion

Catalytic performance tests of $LaCoMn_xO_{(3+\delta)}$ catalysts where x is 0.0, 0.2, 0.3 and 0.5 for the carbon monoxide and ethane oxidation are shown in Figs. 2-3. Ethane was selected as a model for hydrocarbon oxidation. The complete removal of the CO is observed to take place at the range of 150-450°C on different catalysts. Ethane oxidation is also completed over $LaCoMn_{0.3}O_3$ catalyst at 460°C. Removal of the ethane, however, is not completed up to 650°C over $LaCoMn_{(0.2\ or\ 0.5)}O_3$ catalysts. According to the reaction temperature, the results of Figs. 2-3 show that the catalyst with the 0.3 mole manganese added is the best one for the CO and C_2H_6 oxidation; i.e. the complete removal of the CO and C_2H_6 takes place at lower temperature over $LaCoMn_{0.3}O_{(3+\delta)}$ catalyst.

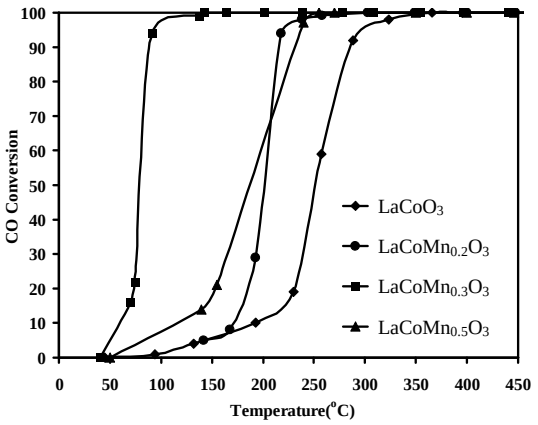

Figure 2. Catalytic performance of $LaCoO_3$, $LaCoMn_{0.2}O_{(3+\delta)}$, $LaCoMn0_{.3}O_{(3+\delta)}$ and $LaCoMn_{0.5}O_{(3+\delta)}$ catalysts for CO oxidation

Representative XRD diffractograms of freshly calcined $LaCoO_3$ and $LaCoMn_{(0.2,\ 0.3\ or\ 0.5)}O_{(3+\delta)}$ catalysts are shown in Fig. 4. XRD patterns of manganese added catalysts are observed to be similar to the $LaCoO_3$ samples. As Fig. 4 shows, manganese oxide is detected to be in the form of the MnO_2 phase. The manganese oxide phase, however, is only observed in the catalysts containing ≥0.3 mole excess manganese. Disappearance of manganese oxide phase in catalysts containing lower than 0.3 mole manganese oxide can be due to low concentration of species in these catalysts. The size of the manganese oxide can also be the other parameter, broadening the XRD peak. According to the XRD results, $LaCoMn_xO_{(3+\delta)}$ catalysts can be proposed as MnO_2 supported lanthanum cobaltite, i.e. $MnO_2/LaCoO_3$.

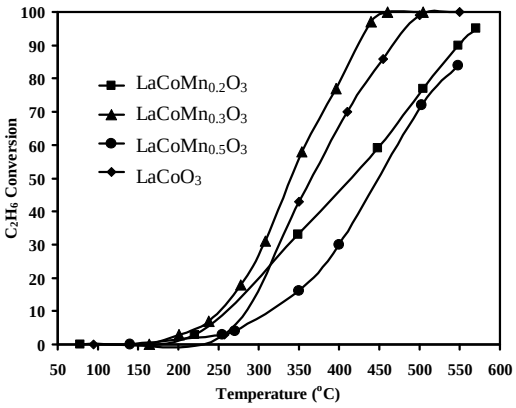

Figure 3. Catalytic performance of $LaCoO_3$, $LaCoMn_{0.2}O_{(3+\delta)}$, $LaCoMn_{0.3}O_{(3+\delta)}$ and $LaCoMn_{0.5}O_{(3+\delta)}$ catalysts for C_2H_6 oxidation

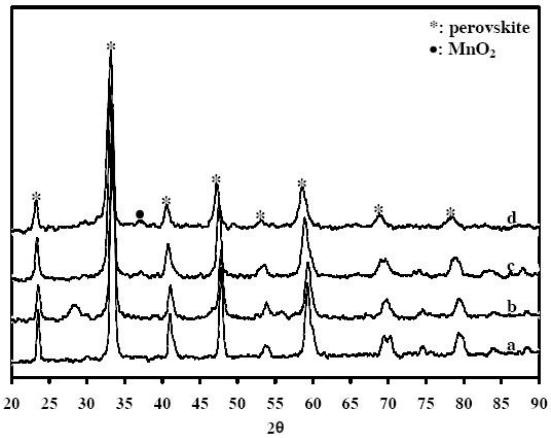

Figure 4. XRD patterns of fresh $LaCoO_3$ (a), $LaCoMn_{0.2}O_{(3+\delta)}$ (b), $LaCoMn_{0.3}O_{(3+\delta)}$ (c) and $LaCoMn_{0.5}O_{(3+\delta)}$ (d) catalysts, calcined at 600°C for 8h

The crystallite size of the perovskite phase, calculated by the Scherrer equation using XRD peaks positioned at 2θ = 23.1, 32.8, 40.5, 47.2 and 58.6° is shown in Table 1. A crystallite size in the range of 13-30 nm is observed for $LaCoMn_{(0.0,\ 0.2,\ 0.3\ or\ 0.5)}O_{(3+\delta)}$ catalysts. Results show that the lanthanum cobaltite perovskite structure is not affected by the manganese addition. A smaller perovskite crystallite size, however, is observed upon manganese oxide addition.

The vibration frequencies in the infrared region are fundamental in the determination of crystalline structures. FT-IR spectra of synthesized perovskites are presented in Fig. 5. The most important band of the perovskites structure corresponds to the asymmetrical lengthening of the B-O bond of the structure's octahedrons BO_6, appearing at 604cm^{-1} [3, 24]. This band appears sharper for the perovskites with more symmetrical structures. The widening of this band and/or the appearance of a shoulder is obtained for structures with lower symmetry. A shoulder at 563cm^{-1} is a characteristic of a rhombohedral structure. Lanthanum cobaltite was reported to have a rhombohedral structure with higher symmetry. A band at 2800 cm^{-1} in $LaCoO_3$ spectrum was assigned to the carbonated segregated La_2O_3 phase.

The FT-IR spectrum for the manganese added lanthanum cobaltite is observed to be the same as that of the $LaCoO_3$ sample (Fig. 5). A broad FT-IR band with a shoulder is evidence of a lower symmetry. In agreement with the XRD pattern, addition of the manganese has no effect on the symmetry. XRD and FT-IR results show the phase segregation does not happen by the addition of manganese.

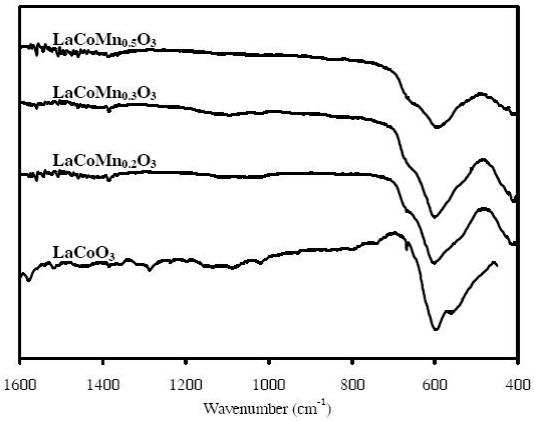

Figure 5. FT-IR spectroscopy results of freshly calcined $LaCoO_3$ (a), $LaCoMn_{0.2}O_{(3+\delta)}$ (b), $LaCoMn_{0.3}O_{(3+\delta)}$ (c) and $LaCoMn_{0.5}O_{(3+\delta)}$ (d) catalysts, calcined for 8 h at 600°C

Table 1. Crystallite size of perovskite phase of the freshly $LaCoMn_{(0.2,\ 0.3\ or\ 0.5)}O_{(3+\delta)}$ catalysts, calcined at 600°C for 8 h.

	Crystallite size (nm)			
2θ	**$LaCoO_3$**	**$LaCoMn_{0.2}O_{(3+\delta)}$**	**$LaCoMn_{0.3}O_{(3+\delta)}$**	**$LaCoMn_{0.5}O_{(3+\delta)}$**
23.1	47	26	26	30
32.8	44	25	23	23
40.5	34	18	18	15
47.2	53	32	29	20
58.6	32	16	15	13
Crystallite size distribution	32-53	16-26	15-26	13-30

The SEM micrographs of fresh $LaCoMn_{0.2}O_{(3+\delta)}$, $LaCoMn_{0.3}O_{(3+\delta)}$ and $LaCoMn_{0.5}O_{(3+\delta)}$ catalysts, calcined at 600°C for 8 h are presented in Fig. 6. In order to show the elemental composition of the samples, the EDS spectra are also included. Surface morphology of the synthesized samples shows no agglomerates in the micro-scale. Another remarkable observation is the appearance of micro-pores in the structure. Results of the FT-IR analysis show that the organic emulsifier, i.e. citric acid, is completely combusted during the heat treatment (see Fig. 5). These pores may be shaped through evolution of the large amount of gases during the calcination process at 600°C. Compared to the catalysts, having 0.2 and 0.5 mole manganese extra, the $LaCoMn_{0.3}O_{(3+\delta)}$ sample is observed to be more porous, resulting in a more active oxidation catalyst (see Figs. 2-3).

The elemental compositions of the catalyst samples determined by EDS analysis are summarized in Table 2. The EDS analysis show the composition is almost the same (within experimental error) as the nominal composition of the samples. The EDS analysis of the composition of different parts of the samples may be an indication of the homogeneity of the prepared catalyst materials in the micro-scale level.

The TEM micrograph of $LaCoO_3$ nanoparticles is shown in Fig. 7. The particle size distribution for this sample, fitted using a gauss function, is presented in Fig. 8. The average particle size for the $LaCoO_3$ sample is calculated to be about 38 nm. This result is in agreement with the calculated crystallite sizes from XRD line profile (see Table 1) and reveals the regularity shape of nano-particles, observed in TEM micrographs [25].

The results of the temperature programmed reduction analysis of $LaCoMn_{(0.2,\ 0.3\ or\ 0.5)}O_{(3+\delta)}$ catalysts are shown in Fig. 9. The TPR profile of $LaCoO_3$ shows two successive reduction peaks, one in the range of 340-480°C and the other in 500-670°C (T_{max} = 600°C) [26]. These successive reduction steps are observed for all $LaCoO_3$ perovskites, as reported by several authors [27-28]. The first reduction peak is described in the literature as a single electron reduction of $Co^{3+} \rightarrow Co^{2+}$ and the second one is attributed to the two electron reduction of $Co^{2+} \rightarrow Co^{0}$.

Table 2. Energy Dispersive Spectroscopy elemental analysis of samples, calcined at 600°C for 8 h.

	$LaCoMn_{0.2}O_{(3+\delta)}$		**$LaCoMn_{0.3}O_{(3+\delta)}$**		**$LaCoMn_{0.5}O_{(3+\delta)}$**	
Element	**N (wt%)**	**M (wt%)**	**N (wt%)**	**M (wt%)**	**N (wt%)**	**M (wt%)**
La	66.52	65.23	64.81	63.03	61.65	58.25
Co	28.22	29.08	27.50	31.14	26.16	29.00
Mn	5.26	5.69	7.69	5.82	12.19	12.75

[a]Nominal
[b]Measured

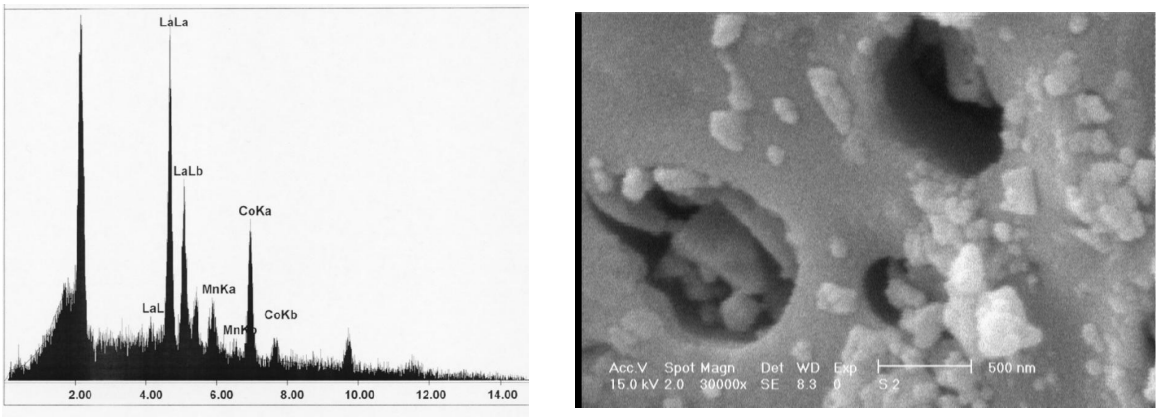

$LaCoMn_{0.2}O_{(3+\delta)}$

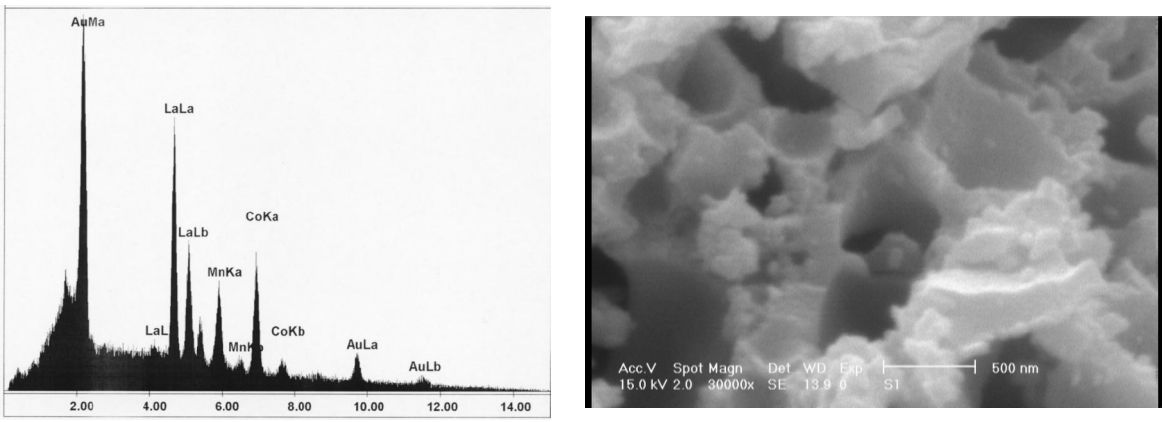

$LaCoMn_{0.3}O_{(3+\delta)}$

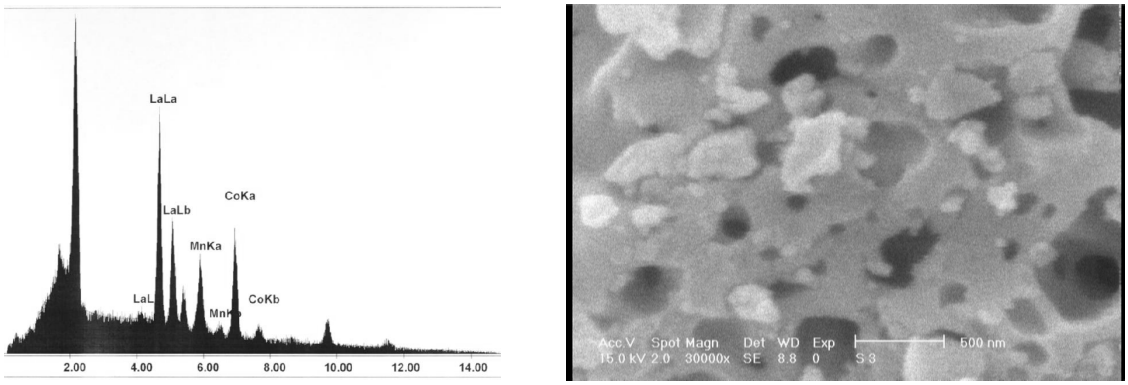

$LaCoMn_{0.5}O_{(3+\delta)}$

Figure 6. Scanning Electron Microscopy (SEM) micrographs and Energy Dispersive Spectroscopy (EDS) elemental analysis spectrum of fresh $LaCoMn_{0.2}O_{(3+\delta)}$, $LaCoMn_{0.3}O_{(3+\delta)}$ and $LaCoMn_{0.5}O_{(3+\delta)}$ catalysts, calcined at 600°C for 8h

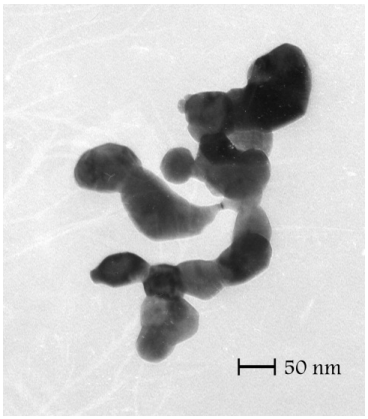

Figure 7. TEM micrograph of $LaCoO_3$ nanoparticles

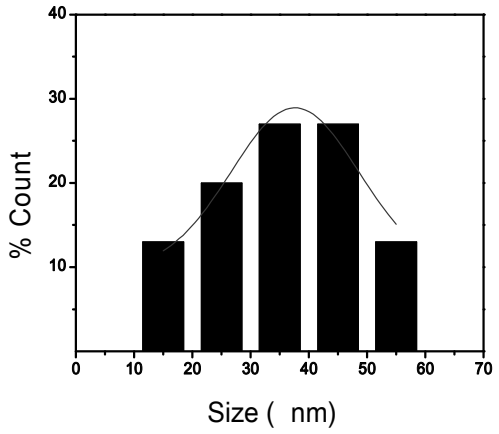

Figure 8. Size distribution histogram for $LaCoO_3$ sample.

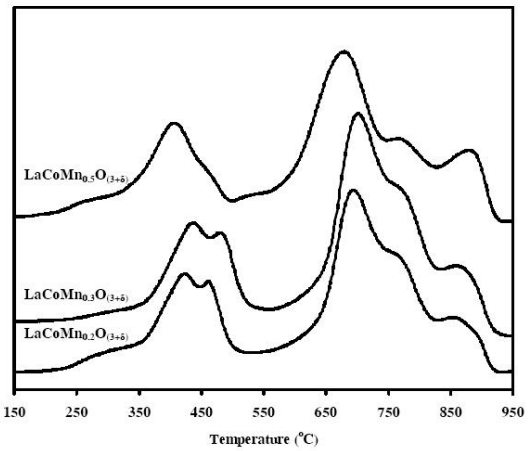

Figure 9. Temperature programmed reduction patterns of fresh $LaCoMn_{(0.2,\ 0.3\ or\ 0.5)}O_{(3+\delta)}$ catalysts, calcined at 600°C for 8 h

The results of Fig. 9 show that presence of the manganese oxide complicates the TPR profile. Assuming a final reduction step to MnO, quantitative data match with an average composition of bulk $MnO_{1.5}$ for samples prepared by direct calcination of the $Mn(NO_3)_2{\cdot}6H_2O$ or $Mn(CH_3COO)_3{\cdot}2H_2O$ precursors, respectively [29]. Reduction patterns of the bulk $MnO_{1.5}$ were associated with the reduction states of $Mn_2O_3 \rightarrow Mn_3O_4 \rightarrow MnO$, respectively [30-33]. Reduction of MnO to metallic Mn was reported to be highly unlikely based on thermodynamic arguments and experimental evidence from the literature [31].

It was proposed that the two cobalt oxide reduction patterns, observed in $LaCoO_3$ TPR, corresponds to the Co_3O_4 reduction in a range of 350-480°C and to cobalt oxide reduction in perovskite structure (range of 550-650°C) [20]. The first reduction in the range of 350-480°C is also observed in the TPR profile of $LaCoMn_{(0.2,\ 0.3\ or\ 0.5)}O_{(3+\delta)}$ sample (see Fig. 9). The reduction in the range of 500-670°C, however, is observed to be harder in the manganese added catalysts. A shoulder in the range of 250-350°C and reduction peaks in the range of 750-900°C are related to the manganese oxide, detected to be MnO_2 by the XRD results. Reduction peaks of the manganese oxide are in agreement with the XRD data. Supported manganese oxide, however, is observed to reduce harder.

4. Conclusions

Addition of the manganese oxide to $LaCoO_3$

perovskite up to 0.3 moles improves the oxidizing property of the sample. A better redox property is observed for $LaCoMn_{0.3}O_{(3+\delta)}$ compared with the $LaCoO_3$ sample. The excess manganese oxide is shown to be in the form of MnO_2 phase. The $LaCoMn_xO_{(3+\delta)}$ catalysts can be shown as MnO_x supported on $LaCoO_3$.

References

[1] Seyfia, B., Baghalhaa, M. and Kazemian, B. H., "Modified $LaCoO_3$ nano-perovskite catalysts for the environmental application of automotive CO oxidation", Chem. Eng. J., Vol. 148, pp. 306-311, (2008).

[2] Radovic, M., Speakman, B. S. A., Allard, B. L. F., Payzantb, E. A., Lara-Curziob, E., Krivenc, W. M., Lloydd, J., Fegelyd, L. and Orlovskayae, N., "Thermal, mechanical and phase stability of $LaCoO_3$ in reducing and oxidizing environments", J. Power Sources., Vol. 184, pp. 77-83, (2008).

[3] Pecchi, G., Campos, C. and Pena, O., "Thermal stability against reduction of $LaMn_{1-y}Co_yO_3$ perovskites", Mater. Res. Bull., Vol. 44, pp. 846-853, (2008).

[4] Bedel, L., Roger, A. C., Estournes, C. and Kiennemann, A., "Co^0 from partial reduction of $La(Co,Fe)O_3$ perovskites for Fischer-Tropsch synthesis", Catal. Today, Vol. 85, pp. 207-218, (2003).

[5] Craciun, R., Nentwick, B., Hadjiivanov, K. and Knözinger, H., "Structure and redox properties of MnO_x/Yttrium-stabilized zirconia (YSZ) catalyst and its used in CO and CH_4 oxidation", Appl. Catal. A-Gen., Vol. 243, pp. 67-79, (2003).

[6] Trawczyn´skia, J., Bielaka, B. and Mis´tab, W., "Oxidation of ethanol over supported manganese catalysts-effect of the carrier", Appl. Catal. B-Environ., Vol. 55, pp. 277-285, (2005).

[7] Kijlstra, W. S., Brands, D. S., Poels, E., K. and Bliek A., "Mechanism of the selective catalytic reduction of NO by NH_3 over MnO_x/Al_2O_3", J. Catal., Vol. 171, pp. 208-218, (1997).

[8] Lamb, A. B., Bray, W. C. and Frazer, J. C., "The removal of carbon monoxide from air", J. Ind. Eng. Chem., Vol. 12, pp. 213-221, (1920).

[9] Kanungo, S. B., "Physicochemical properties of MnO_2 and MnO_2-CuO and their relationship with the catalytic activity for H_2O_2 decomposition and CO oxidation", J. Catal., Vol. 58, pp. 419, (1979).

[10] Nishino, A., "Household appliances using catalysis", Catal. Today, Vol. 10, pp. 107-118, (1991).

[11] Baltanas, M. A., Stiles, A. B. and Katzer, J. R., "Development of supported manganese oxides catalysts for partial oxidation: Preparation and hydrogenation properties", Appl. Catal., Vol. 28, pp. 13-33, (1986).

[12] Wakker, J. P., Gerritsen, A. W. and Mouljin, J. A., "High temperature hydrogen sulfide and carbonyl sulfide removal with manganese oxide (MnO) and iron oxide (FeO) on gamma-

alumina acceptors", Ind. Eng. Chem. Res., Vol. 32, pp. 139, (1993).

[13] Hutchings, G. J., Scurrell, M. S. and Woodhouse, J. R., "Direct partial oxidation of methane: Effect of the oxidant on the reaction", Appl. Catal., Vol. 38, pp. 157-165, (1988).

[14] Hauffe, K. and Ishikawa, Y., "The catalytic oxidation of hydrocarbons in the presence of ozone", Chem. Ing. Tech., Vol. 46, pp. 1053, (1974).

[15] Qi, G. and Yang, R. T., "Characterization and FTIR studies of MnO_x–CeO_2 catalyst for low-temperature selective catalytic reduction of NO with NH_3", J. Phys. Chem. B., Vol. 108, pp. 15738, (2004).

[16] Kramer, M., Schmidt, T., Stowe, K. and Maier, W. F., "Structural and catalytic aspects of sol-gel derived copper manganese oxides as low-temperature CO oxidation catalyst", Appl. Catal. A-Gen., Vol. 302, pp. 257-263, (2006).

[17] Cavallaro, S., Bertuccio, N., Antonucci, P. and Giordano, N., "Mercury removal from waste gases by manganese oxide acceptors", J. Catal., Vol. 73, pp. 337-348, (1982).

[18] Kapteijn, F., van Langeveld, D., Moulijn, J. A., Andreini, A., Vuurman, M. A., Turek, A. M., Jehng, J. M. and Wachs, I. E., "Alumina-supported manganese oxide catalysts: I. characterization: Effect of precursor and loading", J. Catal., Vol. 150, pp. 94-104, (1994).

[19] Imamura, S., Shono, M., Okamoto, A. and Ishida, S., "Effect of cerium on the mobility of oxygen on manganese oxides", Appl. Catal. A-Gen., Vol. 142, pp. 279-288, (1996).

[20] Abadian, L., Malekzadeh, A., Khodadadi, A. A. and Mortazavi, Y., "Effect of excess cobalt oxide nanocrystallites on $LaCoO_3$ catalyst on lowering the light off temperature of CO and hydrocarbons oxidation", J. Chem. Chem. Eng., Vol. 27, pp. 71-77, (2008).

[21] Boaro, M., Giordano, F., Recchia, S., Dal Santo, V., Giona, M. and Trovarelli, A., "On the mechanism of fast oxygen storage and release in ceria-zirconia model catalysts", Appl. Catal. B-Environ., Vol. 52, pp. 225-237, (2004).

[22] Silva, P. P., Silva, F. A., Souza, H. P., Lobo, A. G., Mattos, L. V., Noronha, F. B. and Hori, C. E., "Partial oxidation of methane using $Pt/CeZrO_2/Al_2O_3$ catalysts–effect of preparation methods", Catal. Today., Vol. 101, pp. 31-37, (2005).

[23] Gutierrez-Ortiz, J. I., de Rivas, B., Lopez-Fonseca, R. and Gonzalez-Velasco, J. R., "Combustion of aliphatic C_2 chlorohydrocarbons over ceria–zirconia mixed oxides catalysts", Appl. Catal. A-Gen., Vol. 269, pp. 147-155, (2004).

[24] Baran, E., "Structural chemistry and physicochemical properties of perovskite-like materials", Catal. Today., Vol. 8, pp. 133-151, (1990).

[25] Sertkol, M., Koseoglu, Y., Baykal, A., Kavas, H. and Toprak, M. S.,

"Synthesis and magnetic characterization of $Zn_{0.7}Ni_{0.3}Fe_2O_4$ nanoparticles via microwave-assisted combustion route", J. Magn. Magn. Mater., Vol. 322, pp. 866-871, (2010).

[26] Sartipi, S., Khodadadi, A. and Mortazavi, Y., "Pd-doped $LaCoO_3$ regenerative catalyst for automotive emissions control", Appl. Catal. B-Environ., Vol. 83, pp. 214-220, (2008).

[27] Royer, S., Berube, F. and Kaliaguine, S., "Effect of the synthesis conditions on the redox and catalytic properties in oxidation reactions of $LaCo1\text{-}xFexO_3$", Appl. Catal. A-Gen., Vol. 282, pp. 273-284, (2005).

[28] Engelmann Pirez, M., Granger, P. and Leclercq, G., "Investigation of the catalytic performances of supported noble metal based catalysts in the $NO+H_2$ reaction under lean conditions", Catal. Today, Vol. 107/108, pp. 315-322, (2005).

[29] Arena, F., Torre, T., Raimondo, C. and Parmaliana, A., "Structure and redox properties of bulk and supported manganese oxide catalysts", Phys. Chem. Chem. Phys. (PCCP), Vol. 3, pp. 1911-1917, (2001).

[30] Kapteijn, F., Singoredjo, L., Andreini, A. and Moulijn, J. A., "Activity and selectivity of pure manganese oxides in the selective catalytic reduction of nitric oxide with ammonia", Appl. Catal. B-Environ., Vol. 3, pp. 173-189, (1994).

[31] Trevino, H., Lei, G. D. and Sachtler, W. M. H., "CO hydrogenation to higher oxygenates over promoted rhodium: Nature of the metal–promoter interaction in RhMn/NaY", J. Catal., Vol. 154, pp. 245-252, (1995).

[32] De Jong, K. P., Glezer, J. H. E., Kuipers, H. P. C. E., Knoester, A. and Emeis, C. A., "Highly dispersed Rh/SiO_2 and $Rh/MnO/SiO_2$ catalysts: 1. Synthesis, characterization, and CO hydrogenation activity", J. Catal., Vol. 124, pp. 520-529, (1990).

[33] Stansch, Z., Mleczko, L. and Baerns, M., "Comprehensive kinetics of oxidative coupling of methane over the La_2O_3/CaO catalyst", Ind. Eng. Chem. Res., Vol. 36, pp. 2568-2579, (1997).